AUTOMATIC DETECTION OF RIB CONTOURS IN CHEST RADIOGRAPHS

H. Wechsler and J. Sklansky
Department of Computer Science and School of Engineering
University of California
Irvine, California 92664

Abstract

We have constructed a computer algorithm that finds the contours of the dorsal and ventral portions of the images of ribs in chest radiographs.

The following are a few of the expected uses for the automatic detection of rib contours:

1. Rib images contribute false positives in tumor-detection algorithms. Hence> detecting the rib contours should facilitate removal of these lalse posltives .

2. The ribs provide a frame of reference for the description and location of lesions within the thoracic cavity.

3. The envelope of the ribs provides a more accurate basis for computing the boundary of the chest cavity (referred to as the "lung boundary" In other papers) than other known techniques.

Our algorithtn consists of a) high-pass filtering of the digitized picture, b) local "edge" detection by a combination of thresholding, Laplacian, and gradient operators, c) selection of edge elements in accordance w1th their angular orientation, d) matching straight line segments and conic sect ions to the selected edge elements, e) construct ing strips centered on the straight line segments and conic sections, and f) heuristic search within these strips.

1. _Tntroduction

The delection of the contours of ribs in a radiograph by computer is particularly difficult for a number of reasons.

The optical density changes significantly as one progresses along a contour, and in some instances, parts of a contour disappear. In a chest radiograph, additional problems are imposed by the intersection of the images of ribs, as wel1 as tlie presence of the images of other objects, such as blood vessels or tumors, which may be superimposed in a disturbing way over the sought-after Images of ribs.

The system of algorithms we use for overcoming the above difficulties consists of four major steps, as shown in Figure 1.

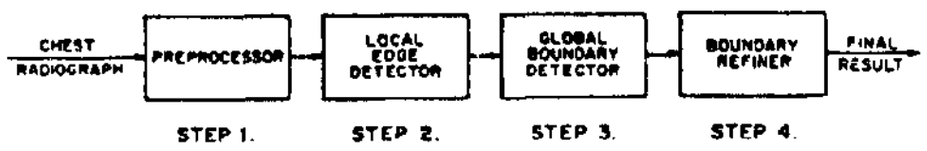

FIGURE 1.' BLOCK DIAGRAM OF RIB CONTOUR DETECTOR

Step 1 digitizes the input picture by an optical scanner and filters the digitized picture by a high-pass digital filter [2, 3]. We refer to this step as a "preprocessor." The input and output pictures of Step 1 are illustrated in Figures 2 and 3, respectively. In these figures the dorsal portions of the ribs are concave downward, and the ventral portions are concave upward. It can be observed in Figures 2 and 3 that the dorsal portions of the ribs are more distinct than the ventral portions. This is a result of the attenuation of X-rays by the lung tissue lying between the dorsal and ventral portions of the rlbs.

Step 2 Is a loca1 edge detect or cons 1stIng of a gradient , a I.aplacian and a threshold ope rat I on.

Step 3 f inds boundaries on a global ha sis by matching conic sections to the contours of the dorsal portions of the ribs and straight line segments to the contours of the ventral portions oi the ribs.

Step 4, the last step, uses the conic sections and the straight line segments of Step 3 as a plan \or obtaining refi tied cont ours . The f 1 na1 result i s shown in Figures H and 9.

Far Her work on automatic rib detection has been reported by TOT iwaki et aj_ [1] . The Ir t echnique, however, a) is restricted to a central strip in each half of the thoracic cage and, within that strip, is effective mainly in the middle subset ot ribs, b) seems to be seriously degraded by tumors and lesions that overlap the rib images, and c) the lower contours of the ventral portions of tinribs are not detected. Our algorithm seems to have none of these weaknesses. In particular, our a Igor i thm has successfully detected ribs that are par t in 11y obscured by a 1arge t umor.

?. I'reproecss i$_n$j»

In our image analysis laboratory the chest radiograph is reduced photographically from 3'i() mm x 430 mm to 100 mm x 125 mm. The reduced picture is digitized by a rotating-drum scanner into a rectangular array of 1024 by 896 8-blt p I - xels, s p a 0.1 mm apart Each pixel is an 8-bit digitization of $\frac{I}{I}$, where I . Is the incident light intensity at a circular spot, and 1 is the t ransmitted 1ight intensity at the spot. The d iameter of the spot is 0.1 mm. To conserve storage space for data and to eliminate some of the noise introduced by the scanner, a consolidation operation is performed. The consolidation operation replaces every 4-by-4 square array of pixels in the digitized picture by the average of the picture function in that array, thereby reducing the size of the digital picture to 256 by 224 pixels. Figure 2 displays the digitized picture after scanning and consolidation.

To enhance the edges, a high-pass filtering in the spatial frequency domain is carried out.

using the Fast Fourier Transform [3] and a transform function suggested by Kruger [2].

Let ω denote the modulus of the two-dimensional vector of angular spatial frequencies in the Fourier transform of p(x). Let ω_c and ω_T denote the angular frequencies below which lie 0.99 and 0.9995, respectively, of the spectral energy of p(x). Let f denote the sampling frequency - i.e., the reciprocal of the spacing between adjacent pixels. (In our case f is 2.5 lines/mm.) Let

$$\lambda = 3 + 2\left(\frac{\omega_T - 0.2f_o}{0.2f_o}\right)$$

In terms of these quantities, the transfer function $H(\omega)$ of our high-pass filter is

$$H(\omega) = \begin{cases} 1 \text{ for } \omega \leq \omega_c \\ \lambda\left[1 - \left(\dfrac{\omega_T - \omega}{\omega_T - \omega_c}\right)^2\right] \text{ for } \omega_c < \omega < \omega_T \\ \lambda + 1 \text{ for } \omega \geq \omega_T \end{cases}$$

The rationale behind this high-pass filtering is that high spatial frequencies are due primarily to sharp changes in gray-level densities, i.e., to the edges present in the picture.

The digitized chest radiograph obtained by the high-pass filtering operation is illustrated in Figure 3.

3. Local Edge Detection

The rib contours are smoothed, low-curvature curves and hence may be approximated by a chain code [10]. We refer to each element of this chain as a locfll edge element. The detection of local edge elements is a major task in the detection of rib contours because the vascular tissue deteriorates the sharpness of the local edges. As a result, only edge elements that satisfy several criteria simultaneously are selected by our algorithm.

Our local edge detector, described below in detail, consists of a) the modulus and the direction of a digital approximation of the spatial gradient, b) a digital approximation of the Laplacian, and c) thresholds applied to the results of the gradient and the Laplacian operations.

3.1 Computation of the Gradient

The picture of the modulus of the gradient is computed by Eqs. 3-1 through 3-3. Here p(i,j) denotes the digitized measurement of $y \log (I/I_o)$ at pixel (i,j), G(i,j) denotes the modulus of the digital approximation of the gradient at (i,j), and y is a constant.

$$\Delta_x(i,j) = 2[p(i,j+n) - p(i,j-n)] + [p(i+n,j+n) - p(i+n,j-n)] + [p(i-n,j+n) - p(i-n,j-n)] \quad (3\text{-}1)$$

$$\Delta_y(i,j) = 2[p(i-n,j) - p(i+n,j)] + [p(i-n,j-n) - p(i+n,j-n)] + [p(i-n,j+n) - p(i+n,j+n)] \quad (3\text{-}2)$$

$$G(i,j) = \sqrt{\Delta_x^2(i,j) + \Delta_y^2(i,j)} \quad (3\text{-}3)$$

The variable n specifies how far apart on the picture grid the differences are taken. The quantity 2n+1 is referred to as the span of the gradient. We found that n = 1 is best for our data. The gradient modulus picture provides us with knowledge about the existence of edges, but it does not take account of their direction. This directional information plays an important role in subsequent parts of our system. The direction is information from which we can infer connectivity. Thus two adjacent edge elements are very likely to lie on the same continuous curve (i.e., rib contour) if they have almost the same direction. The direction at pixel (1,1) is defined as:

$$D(i,j) = \tan^{-1}\frac{\Delta_y(i,j)}{\Delta_x(i,j)} \quad (3\text{-}4)$$

where $\Delta_x(i,j)$, $\Delta_y(i,j)$ were defined by Eqs. 3-1 and 3-2, respectively.

We quantize this direction to one of the four Cartesian quadrants, Q(i,j). Specifically,

$$Q(i,j) = k \text{ such that } \frac{k\pi}{2} \leq D(i,j) < (k+1)\frac{\pi}{2} \text{ and } k \in \{1,2,3,4\} \quad (3\text{-}5)$$

Thus the gradient operation provides us with the following information at each pixel (i,j) of the grid: G(i,j), D(i,j), and Q(i,j).

3,2 Computation of the Laplacian

Many digital approximations of the Laplacian have been proposed [6]. We computed the magnitude of the Laplacian by Eq, (3-6). Here L(i,j) denotes the Laplacian calculated at pixel (i,j):

$$L(i,j) = |4p(i,j) - (p(i,j-1) + p(i,j+1) + p(i+1,j) + p(i-1,j)| \quad (3\text{-}6)$$

3.3 Thresholding and Directional Maps

After we performed the operations described in sections 3.1 and 3.2, we have for each pixel (i,j) the following information: G(i,j), Q(i,j), and L(i,j).

The thresholding portion of the local edge detector uses two thresholds Θ_G and Θ_L to produce a binary picture M(i,j) defined by

$$M(i,j) = \begin{cases} 1 \text{ if } G(i,j) > \Theta_G \text{ and } L(i,j) > \Theta_L \\ 0 \text{ otherwise} \end{cases} \qquad (3\text{-}7)$$

The reasons why both the gradient and the Laplacian are needed are as follows:

a) the gradient does not take account of the gray-level at the pixel itself, whereas the Laplacian does;

b) the edges of the picture function depend primarily on the first two derivatives of the picture function; and

c) it has been shown that the eye can detect only low-order derivatives.

The picture M(i,j) contains information about where reliable edges exist in the given picture, A direction picture R(i,j) is built from the binary picture M(l,j) by replacing each 1 in M(i,J) fi.e., each edge element) by its quadrant 0(1,j). Thus,

$$R(i,j) = M(i,j)\, Q(i,j) \qquad (3\text{-}8)$$

Figure 4 shows the output of Step 3, where $\Theta_G = 150$ and $\Theta_L = 30$. Here we display only the lower boundaries of the ribs in the right and left lung,i.e., those pixels where the gradient modulus and Laplacian are bigger than prespecifled thresholds. The directional picture R(i,J) is represented in our figure by fish-shaped edge elements "swimming" in the direction of the boundaries. As the "fish swims" it sees on its left a region of greater light intensity than on its right.

The edge elements of the lower boundaries in the right lung are characterized by quadrant Q = 3, whereas the edge elements corresponding to the lower boundaries in the left lung are characterized by quadrant Q = 2. Figure 5 displays a window taken from the right lung, showing Images of dorsal and ventral ribs intersecting.

4. Global Boundary Detector

The edge elements produced by Step 3 have three principal shortcomings as respresentatives of the rib contours: 1) some portions of the contours are represented by overly thick "roads," 2) some portions of the contours are not represented at all, i.e., there are gaps in the contour estimates, and 3) a few edge elements are not true edge elements and thus constitute noise.

The function of the global boundary detector is to overcome all three of these shortcomings: 1) it thins the thick portions, 2) it fills the gaps, and 3) it eliminates the noise.

The global boundary detector is a curve fitting procedure similar in concept to the Hough line detector [5]. Each pixel in M(i,J) is transformed into a curve in a new parameter space, p* Every point on this curve in p-space uniquely represents a specific curve passing through (i,j) in the original (i,,j)-space. We call this procedure an accumulator array procedure, because we can think about the p-space as a d-dimensional array and each cell in this array accumulates the number of pixels where M(i,j) - 1 and which lie on the same curve in (i,j)-space.

We applied the Hough technique of detecting straight lines to the images of the ventral ribs. In the picture shown by Figure 3, we can distinguish seven ventral ribs (fourteen contours) in the right lung and six ventral ribs (twelve contours) in the left lung. From the total of twenty-six contours, twenty-one were found directly from the Hough detector, two ambiguities were solved based upon the thickness of the surrounding ventral ribs, one correction was made based upon the approximate thickness of a ventral rib, and two contours which were missed by the Hough detector due to the absence of enough relevant points were found by an extrapolation from the thickness and the location of the neighboring ventral ribs.

To find the contours of the dorsal portions, ve extended the Hough concept to the detection of conic sections (parabolas and ellipses). We assumed that the images of the dorsal rib contoura can be approximated by conic sections, and that each of these conic sections has a maximum ordinate with a zero derivative. We applied an accumulator array procedure which detects small regions within the rib cage which are most likely to contain the foci of the conic sections. This algorithm uses the relationship between the points on the conic sections and the parameters of these curves. From the gradient direction at a given pixel (i,j), we compute a small range of admissible directions for the conic sections passing through that pixel. We use the range of directions rather than the single computed direction of the gradient in order to overcome the effects of noise and quantization. Consider the pixels obtained by Step 2 and having the configuration $(Q,\delta) * (1,1)$ or (3,1) where 0 * quadrant and $\delta = 1$ for the right lung and $\delta = 2$ for the left lung. For each of these pixels, our system computes the foci of conic sections passing through the pixel and having the directions in the range defined above. I.e., our system computes those conic sections whose D(i,j) belongs to the computed range.

The array of accumulators is initialized at the value zero. Each elementary computation finds a possible focus (a,b) and increases the contents of the corresponding accumulator by 1. Eventually the algorithm provides us with high-valued accumulator cells. These cells are the foci of the most

likely conic sections lying on the boundaries. These conic sections are then constructed by our system of algorithms.

Exploiting symmetry along the sternum (breast bone), we use the same program for both the right and the left lung. The maximum ordinates were found by using accumulator array techniques to detect short horizontal line segments. Ambiguities due to the hilar region were solved based upon the surrounding dorsal ribs.

5. Refinement of Rib Boundaries

In a session dedicated to Robot Problem Solving at the 1973 IJCAI, Sacerdotl pointed out that a problem domain can be represented as a hierarchy of abstraction spaces in which successively finer levels of details are introduced [9]. The rationale behind this hierarchy of abstraction spaces is that in order to be efficient, our problem solvers need to make extensive use of different heuristics at different stages of our problem-solving process [5]. Examples of implementations of this concept are the top-down programming approach as well as the "THE" operating-system of Dijkstra [8]. Our system of algorithms exploits such a rationale.

Step 3 approximates the rib contours by conic sections and straight line segments. In Step 4 small strips are centered around the curve segments found by Step 3. These strips constitute a "plan" in the sense of Ballard-Sklansky [12]. By using a heuristic function h, with a small look-ahead, we fit the best curve to the rib contours. Subsequently, a smoothing algorithm provides us with a smoothed curve. In this way we find a rough approximation of the rib contours at a higher level and we introduce the details at a lower one.

Now we will describe Step 4 in detail. In particular, we will answer the following question. From a pixel (i,J) on the rib boundary, how does Step 4 choose the next pixel by using the heuristic function h?

Step 4 operates as follows. A small tree with a look-ahead of three is built having the pixel (l,j) at its root and all the paths through this tree are evaluated.

We then choose as the next pixel on the curve that successor of (i,j) such that a maximum accumulation of h is achieved for a path passing through (i,j).

h(i,J) is defined as follows:

$$h(i,j) = \begin{cases} G(i,j) + \alpha L(i,j) - \beta_1 - \beta_2 & \text{if the set of conditions } \{C_j\} \text{ holds} \\ 0 & \text{otherwise} \end{cases}$$

In the above definition G(i,j) and L(i,,j) are the magnitude of the gradient and of the Laplacian respectively, a being constant (usually 3). fr is a penalizing constant which is zero for points located In the middle of the strip and is increasing as we approach the border of the atrip. The use of $, forces the path to lie within the desired atrip. As we go along the refined rib contour, new information is gained and a new and Improved plan could be built. Baaed upon the last pixel added to the rib contour and the location along the same contour, a next pixel can be predicted. The effect of Ba is to keep us as close ae possible to this next predicted pixel.

{C.} la a set of conditions which assures us that the pixel (i,j) can be located on the curve we are looking for. The conditions (Cj) are the following:

C_1 (i.j) belongs to the configuration (Q,6) we are looking for,

C_2: by choosing (i,j) the connectivity criterion is satisfied,

C_3: the curve which is going to pass through (i,J) is going to be a monotonically nondecreasing function up to the maximum location of the dorsal rib and afterwards a monotonically nonincreasing function until it reaches the lung boundary, and this should hold for the image of a dorsal rib contour, and

C_4: the curve which is going to pass through (i,j) is going to be a monotonically nonincreasing function for the Images of the ventral ribs.

Termination conditions as boundary pixels are provided. In the case of the images of the ventral ribs, we stop going along the contour when there is a lack of pixels showing the triplet corresponding to the ventral contours and where supposedly the costal cartilages are starting.

Figure 7 shows the effect of this processor on the image of a ventral rib contour.

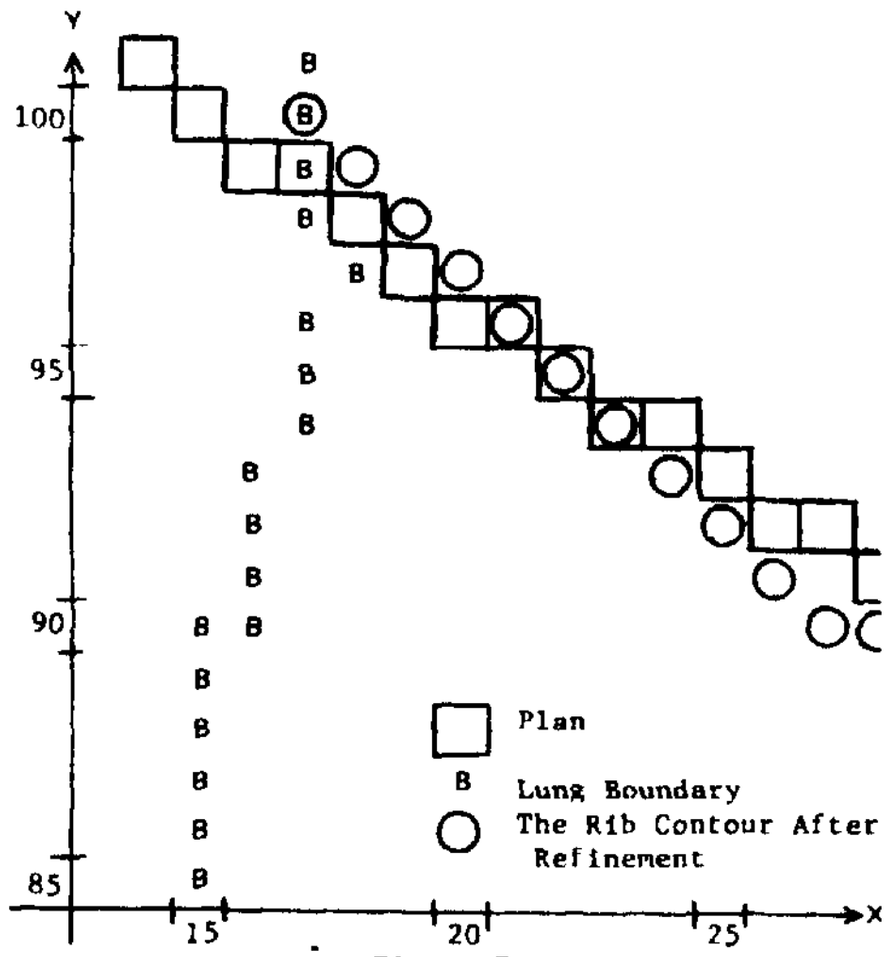

Figure 7
Refinement of a Ventral Rib Contour

Figure 6a, b, c displays the effect of Step 4 on two intersecting rib contours (a dorsal and a ventral one). We can distinguish the plan obtained by the third step, the rib contours, after refinement using h, and finally the same rib contours after smoothing. The pictures have been recorded at a magnification of 2 in order to display the results more clearly (i.e., each pixel is shown as a 2 x 2 matrix). Figures 8 and 9 show the result of applying Step 4 to the output of Step 3. This is also the final output for the input shown in Figure 2.

Earlier use of heuristic curve following has been reported by Martelli [13] and Ballard-Sklansky 112], but to our best knowledge, this is the first use of look-ahead in heuristic curve following.

6. Summary and Concluding Remarks

The automatic detection of rib images in a chest radiograph requires a sophisticated system of algorithms. In this paper we describe such a system. One of the special attractions of our system is that it can be implemented effectively on a small computer (a "minicomputer") having only eight thousand 16-bit words of core memory and 2.5 million 16-bit words of disc memory. This paper also •hows how several concepts of artificial intelligence have contributed to establishing the feasibility of a system of algorithms for a difficult task In machine vision. (One must recognize that "difficulty" depends on the sophistication of the problem solver. A "difficult" problem often becomes "easy" after one becomes familiar with Its solution.)

The rib contours detected by our system agree closely with our perception of these contours.

Improvaments in our technique for rib detection may lie along the following directions! 1) texture analysis of lung tissue and the bone struc-*-ture of ribs, 2) building an explicit world-model representation of the rib cage, and 3) computer-radiologist interaction.

7. Acknowledgments

This research was supported by the National Institute of General Medical Sciences of the U.S. Public Health Service under Grant No. GM-17632.

We are grateful to Dr. B. J. O'Loughlin of the University of California, Irvine, College of Medicine for his comments and discussions.

8. References

1. Toriwaki, J., Suenaga, Y., Negoro, R., Fukumura, T., "Pattern Recognition of Chest X-ray Images," Computer Graphics and Image Processing, Vol. 2, No. 3/4, December 1973.

2. Kruger, R. P, "Computer Processing of Radiographic Images," Ph.D. Dissertation, Engineering Department, University of Missouri, Columbia, 1971.

3. IEEE Transactions on Audio and Electroacoust_lca (1967), AU-15, No. 2, June 1967.

4. Tenenbaum, J. M., "On Locating Objects by Their Distinguishing Features in Multisensory Images," A. I. Center, Technical Note 84, SRI Project.

5. Duda, R. 0., Hart, P. E., "Use of the Hough Transformation to Detect Lines and Curves in Pictures," Comm. of ACM, January 1972, Vol. 15, No. 1.

6. Rosenfeld, A., Picture Processing by Computer, Academic Press, New York, 1968.

7. Sacerdoti, E. D,, "Planning in a Hierarchy of Abstraction Spaces," IJCA1 1973 Proceedings-

8. Dljkstra, E. W., "The Structure of the "THE" Multiprogramming System," Comm. of the ACM, May 1968.

9. Nilsson, N. J., Problem Solving in Artificial Intelligence. McGraw-Hill, 1971.

10. Freeman, H., "On the Encoding of Arbitrary Geometric ConfigurationB," IRE Transactions, EC-10, Vol. 2, pp. 260-268, June 1961.

11. Martelli, A., "Edge Detection Using Heuristic Search Methods," Computer Graphics and Imape Processing, Vol. 1, No. 2, August 1972.

12. Ballard, D. H., Sklansky, J., "A Ladder-Structured Decision Tree for Recognizing Tumors in Chest Radiographs," TP-74-8, University of California, Irvine, 1974.

Figure 2
Digitized Picture Before
High-Pass Filtering.

Figure 3
Digitized Picture After
High-Pass Filtering.

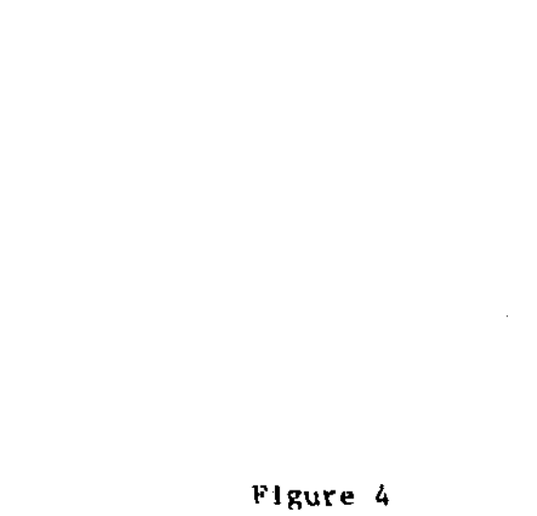

Figure 4
Direction Map Displaying the Lower
Boundaries of the Ribs in the
Right and Left Lung.

Figure 5
Direction Map Displaying
Dorsal and Ventral Ribs
Intersecting in the
Right Lung.

Figure 6a
Before Refinement.

Figure 6b
After Refinement Using
Heuristic Search.

Figure 6c
After Smoothing

Figure 6
Dorsal and Ventral Rib Contours
Before and After Using Heuristic Search

Figure 8
Dorsal Rib Contours
Final Result.

Figure 9
Ventral Rib Contours
Final Result.